Composites Science and Technology 74 (2013) 166–172

Contents lists available at SciVerse ScienceDirect

Composites Science and Technology

journal homepage: www.elsevier.com/locate/compscitech

Latex and two-roll mill processing of thermally-exfoliated graphite oxide/natural rubber nanocomposites

Jeffrey R. Potts[a], Om Shankar[a], Shanthi Murali[a], Ling Du[b], Rodney S. Ruoff[a,*]

[a] Department of Mechanical Engineering and the Materials Science and Engineering Program, The University of Texas at Austin, 204 E. Dean Keeton St., Austin, TX 78712, USA
[b] Goodyear Tire & Rubber Company, 1144 E. Market St., Akron, OH 44316, USA

ARTICLE INFO

Article history:
Received 15 May 2012
Received in revised form 9 October 2012
Accepted 15 November 2012
Available online 23 November 2012

Keywords:
A. Nano composites
A. Polymer–matrix composites (PMCs)
C. Transmission electron microscopy (TEM)

ABSTRACT

Thermally-exfoliated graphite oxide (TEGO) is a graphene-based material that has been previously shown to disperse effectively into thermoplastic polymers by melt processing. In this work, dispersion of TEGO into natural rubber (NR) directly on a two-roll mill did not result in substantial property enhancement. However, by pre-mixing the TEGO with NR latex by an ultrasonically-assisted latex co-coagulation procedure followed by two-roll milling, the properties were improved substantially over the TEGO/NR nanocomposites mixed only on the mill. Quantitative analysis of TEM micrographs suggested the difference in properties was primarily the result of improved dispersion, as fewer multi-layer tactoids and platelets of overall smaller dimensions were observed in the nanocomposites pre-mixed by latex co-coagulation. NR filled with carbon black showed comparable property enhancement to TEGO/NR mixed on the two-roll mill but much smaller property changes than the latex pre-mixed TEGO/NR nanocomposites.

1. Introduction

The exceptional physical properties and high aspect ratio structure of graphene-based materials offer great potential for multifunctional property enhancement of polymer materials [1]. A continuing challenge in this rapidly-growing field is to find effective methods for dispersion of graphene platelets into polymers. To date, however, relatively little work has been done on mixing of graphene-based materials into non-polar rubbers such as natural rubber (NR) that are widely used for critical applications, e.g., tires [2,3].

Graphite oxide (GO) is the typical precursor to graphene-based materials [4]. GO can be exfoliated in water into single-layer graphene oxide platelets and subsequently reduced (i.e., deoxygenated) to yield a colloidal suspension of graphene-like platelets. GO can also be exfoliated by heating—the resulting material, called thermally-exfoliated graphite oxide (TEGO), resembles graphene on a local scale but contains defects such as holes. TEGO is produced by heating GO to high enough temperatures (300 °C or higher [5]) to drive off interlamellar water and initiate decomposition of surface functional groups, which generates internal pressure sufficient to push the layers apart and expand the material into an accordion-like structure of loosely-stacked platelets [6]. Microwave irradiation or mechanical shock of GO can also produce materials similar to TEGO [7]. Fig. 1 illustrates the relationship between GO and these graphene-based materials.

From Fig. 1, it is helpful to distinguish two distinct classes of graphene-based materials. One consists of TEGO and microwave-exfoliated graphite oxide (MEGO) which are produced by thermal exfoliation and in bulk form are dry, fluffy powders with a low bulk density. The other includes reduced graphene oxide and other chemically modified graphene materials, which are generally handled in colloidal suspensions. Previous work suggests that the class of graphene-based material has implications for the relative effectiveness of the typical nanocomposite dispersion method(s) [1]. For instance, colloidal suspensions of graphene platelets can be agglomerated to yield dry powders and subsequently mixed with a polymer via melt processing [8,9], but attempts to disperse graphene platelets in this manner have yielded poor results [2,10] to date despite melt processing being highly effective for dispersion of TEGO. Conversely, it is apparently difficult to form homogeneous colloidal suspensions of TEGO in solvents, affording a relatively poor dispersion if mixed into polymers by solution blending processes [11].

Recently, we reported on the formation of reduced graphene oxide (RG-O)/NR nanocomposites by co-coagulation of RG-O colloidal suspensions and NR latex, which resulted in exceptional multifunctional property enhancement of the NR [12]. In this work, we sought to evaluate the effectiveness of a “melt” compounding approach, using conventional rubber processing equipment, for dispersing TEGO into NR. This problem is of industrial significance as fillers such as carbon black are generally dispersed into

---

[*] Corresponding author. Tel.: +1 512 471 4691.
E-mail address: r.ruoff@mail.utexas.edu (R.S. Ruoff).

0266-3538/$ - see front matter © 2012 Elsevier Ltd. All rights reserved.
http://dx.doi.org/10.1016/j.compscitech.2012.11.008

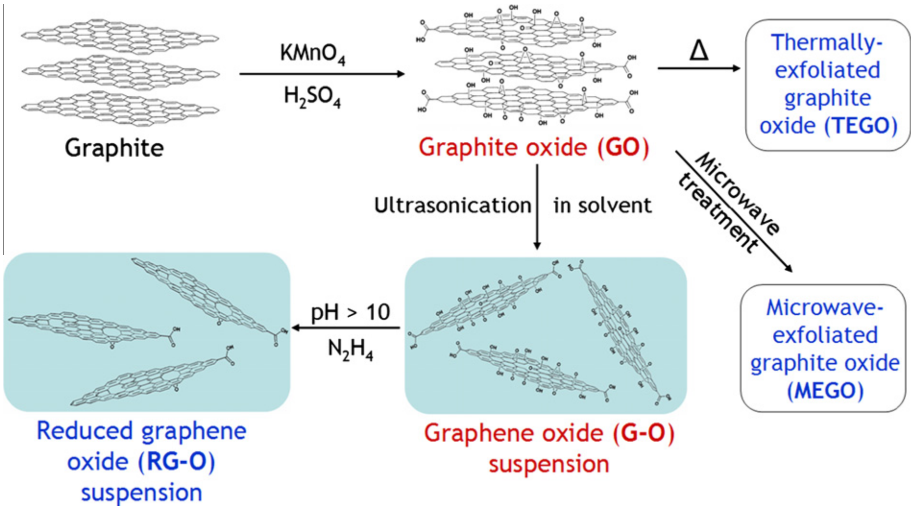

Fig. 1. Schematic showing production routes for graphene-based materials from graphite oxide (GO).

elastomers without the use of solvents, using mixing equipment such as an internal (Banbury-type) mixer or, for smaller compounding operations, a two-roll mill [13].

However, our preliminary measurements on nanocomposites produced by direct milling of TEGO into NR showed small property enhancements relative to our recent work with RG-O/NR nanocomposites. In an attempt to improve properties further, we used ultrasound-assisted latex compounding to mix master batches of TEGO and NR prior to two-roll milling to break down the TEGO particles prior to milling. In this paper, we evaluate the effectiveness of these processing approaches by comparing the morphology and properties of the two sets of TEGO/NR nanocomposites to each other and to NR filled with carbon black.

2. Experimental

2.1. Filler preparation, nanocomposite production and processing

GO was produced using a modified Hummers method [9,12]. To produce TEGO, GO was added into a 1 L beaker covered with aluminum foil on a hot plate set at 400 °C; this caused rapid expansion of the GO to yield a fluffy, black powder. The powder was collected from the beaker and dried for at least 24 h in a vacuum oven at 40 °C prior to use. Carbon black (CB) from Alfa Aesar was used in this study, with a specific surface area of 50 m^2/g according to the manufacturer. Natural rubber (NR) latex was provided by Goodyear Tire & Rubber Company. Dicumyl peroxide (DCP, 98%) was used as-received from Aldrich. NR latex was coagulated with 5 vol.% formic acid (Aldrich) and dried for use in milling experiments. Latex "pre-mixing" was achieved by adding TEGO powder to water (approximately 1 g in 1 L), treating on an ultrasonic bath for ~20 min with stirring, addition of NR latex and stirring/sonicating for 20 min, followed by co-coagulation with formic acid.

A two-roll prep mill (4″ × 8″ rolls, CW Brabender Instruments) was used for the mixing of filler and curing agent. The rolls were set to a temperature of approximately 60 °C, a speed of 15 RPM with a friction ratio of 1.3:1, and a nip gap of 1 mm. For each 5 part per hundred rubber (phr) masterbatch, a sufficient quantity of NR or composite was used to allow complete banding on the roll (>50 g). A total milling time of 10 min was used for dispersion of filler into NR (10 min was also used for the pre-mixed nanocomposites). It should be noted that the low bulk density of TEGO makes it susceptible to becoming airborne and flying away from the mill rather than mixing into the rubber. To address this issue, the TEGO was compressed by hand into pellets that were charged into the mill. After addition of filler, the nanocomposite was cut from the mill and weighed to ensure that the mass had increased by the required amount. Portions of the 5 phr masterbatches were diluted with neat NR to achieve lower loading levels; at this stage DCP was added at a concentration of 1 phr. Milling time for dilution and DCP incorporation was approximately 10 min, for a total milling time of 20 min. 5 phr nanocomposites and neat NR batches were also milled for a total of 20 min. The nanocomposites were molded and cured in a Wabash hot press at 150 °C for 50 min under a 40 kip load.

2.2. Morphological characterization

Transmission electron microscopy (TEM), scanning electron microscopy (SEM), and wide angle X-ray scattering (WAXS) were used to characterize filler or nanocomposite morphology. For TEM imaging, thin sections (~70 nm) of composite were prepared using a cryo-ultramicrotome (Leica Inst., DiATOME cryo 35° diamond blade) with a −120 °C chamber temperature and a knife temperature of −95 °C. The thin sections were collected onto 300 mesh Gilder grids from Ted Pella. TEM digital micrographs were acquired using a JEOL 2010F at 200 kV. SEM images were obtained using an FEI Quanta-600 FEG Environmental SEM at 20 kV and 10^{-6} torr. X-ray scattering was performed on a Philips X-PERT diffractometer using Cu Kα radiation, a generating voltage of 40 kV, a current of 30 mA, and a 2 s dwell time.

2.3. Stress–strain testing and dynamic mechanical analysis

Uniaxial tensile testing was performed at room temperature with an MTS machine equipped with a 25 lb Honeywell load cell and spring-loaded clamps to prevent specimen slippage. Data was acquired using LabVIEW. Samples were "dog-bone" shaped with approximate test section dimensions of 20 × 4 × 1 mm. Milled samples were stretched at least five times to an elongation of 200% prior to testing to correct for stress softening (Mullins effect [14]). The strain rate for all tests was 500 mm/min. Dynamic mechanical analysis (DMA) was performed using a TA Instruments Q800 DMA. All tests were conducted at 10 Hz from −100 °C to 50 °C with a ramp rate of 3 °C/min, a strain of 0.1%, and a static preload of 0.01 N. Samples had dimensions of approximately 15 × 5 × 1 mm.

2.4. Thermal and electrical conductivity testing

Electrical conductivity measurements were made using a HIOKI Ultramega ohmmeter (SM-8220) with a HIOKI SM-8000 series electrode and enclosure; samples were disk-shaped and ~1 mm thick with a surface area (of one face) of at least 1 cm^2. The in-plane thermal conductivity was measured by Goodyear Tire & Rubber Company using a transient hot disk method; samples measured 51 mm × 51 mm × 6.4 mm. The thermal conductivity was calculated from the measured density, specific heat, and thermal diffusivity.

2.5. Filler analysis

XPS analysis was performed using a Kratos AXIS Ultra DLD spectrometer (monochromated Al K emission at 1486.6 eV with an operating power of 150 W). Determination of specific surface area using the Brunauer–Emmett–Teller (BET) equation was carried out on a Quantachrome Instruments Nova 2000 using nitrogen as the adsorbent at 77 K.

3. Results and discussion

3.1. Properties of TEGO

Fig. 2 shows SEM micrographs of TEGO particles, revealing the "accordion-like" structure of the material consisting of highly wrinkled and exfoliated graphene-like platelets loosely stacked together. The TEGO material used in this study had a BET surface area of 454 m^2/g and a C:O ratio of 4:1, as determined by X-ray photoelectron spectroscopy (see Fig. A1). This C:O ratio is lower than reported elsewhere for TEGO and may be due to the exfoliation temperature of 400 °C used in this study, as many other reports use temperatures of 1000 °C or more to produce TEGO [6,15]. The lower processing temperature was chosen for more rapid production of larger quantities (~10 g) of TEGO in a glass beaker compared with tube furnace exfoliation and annealing at higher temperature. The lower processing temperature may have facilitated dispersion of TEGO into water during the latex pre-mixing step, but the relatively high oxygen content on this TEGO may have also been detrimental to the nanocomposite properties as NR is a non-polar polymer.

3.2. Nanocomposite properties

The high modulus and high aspect ratio of graphene-based materials confers significant modulus and strength improvements to polymers if properly dispersed. Several previous studies have demonstrated the effective dispersion of TEGO [8] and related materials [9] into various polymer matrices by melt compounding. Moreover, recent work has reported on the effective dispersion of layered silicates into NR by two roll mill processing [16]. In light of these results and the presumed thermodynamic compatibility between graphene-based materials and NR [3,12], it was hoped that two-roll mill processing would lead to excellent dispersion of TEGO. However, the expected property improvements were not realized by this dispersion method alone. On the other hand, significant increases in modulus and strength were observed in TEGO/NR nanocomposites subjected to a latex "pre-mixing" step (henceforth, L-TEGO/NR). Fig. 3 shows stress–strain curves from the two types of TEGO/NR nanocomposites.

Fig. 4 summarizes mechanical property data over the range of loadings tested. The modulus at 100% elongation (M100) and at 300% elongation (M300) of the TEGO/NR nanocomposites decreased relative to neat NR at 2 phr and 3 phr loading, with small increases over neat NR with 4 and 5 phr TEGO. Conversely, at just 2 phr, M100 of the L-TEGO/NR nanocomposites was 38% higher than the M100 of the 5 phr TEGO/NR nanocomposites. Differences in M300 enhancement were particularly pronounced between the two types of nanocomposites. Mirroring the trends observed in RG-O/NR nanocomposites [12], the L-TEGO/NR nanocomposites showed increasing tensile strength but decreasing strain at break with increasing TEGO loading.

The enhancement of electrical conductivity in polymer nanocomposites is strongly dependent upon the filler morphology; the formation of percolating pathways between filler particles is necessary to render an insulating polymer such as NR electrically conductive [17]. Previously, our work with RG-O/NR nanocomposites showed maximum enhancement in conductivity not when the filler was homogeneously dispersed, but rather arranged into a connected "web-like" structure of platelets [12]. In this study, both processing approaches led to homogeneous filler dispersions, and consequently the electrical conductivity of these TEGO nanocomposites was lower than in our previous work. For homogeneous dispersions as produced by mill processing [12], more well-exfoliated platelets should result in maximum conductivity enhancement [18]. As shown in Fig. 5, the L-TEGO/NR nanocomposites exhibited higher conductivity both in and out of the sample plane, suggesting a better dispersion or higher average aspect ratio of the dispersed platelets compared with the TEGO/NR nanocomposites.

Fig. 6 shows Mooney–Rivlin plots of reduced stress σ^* versus reciprocal extension ratio α based on the selected stress–strain curves presented in Fig. 3. The upturn in σ^* shifts to lower $1/\alpha$ values with higher loading as a result of promotion of strain-induced crystallization by the presence of the filler [2,3]; this trend is

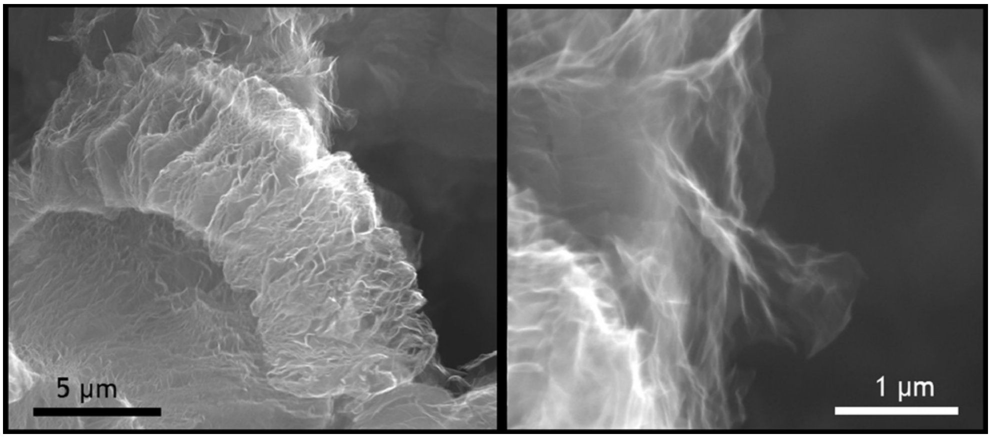

Fig. 2. SEM micrographs of TEGO particles produced by thermal expansion of GO, showing the presence of wrinkled platelets arranged into an accordion-like structure.

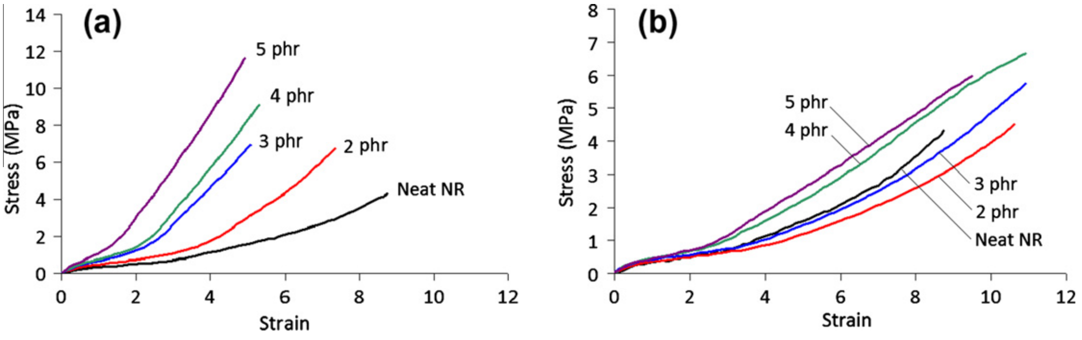

Fig. 3. Representative stress–strain curves of (a) L-TEGO/NR nanocomposites and (b) TEGO/NR nanocomposites, each at various loadings.

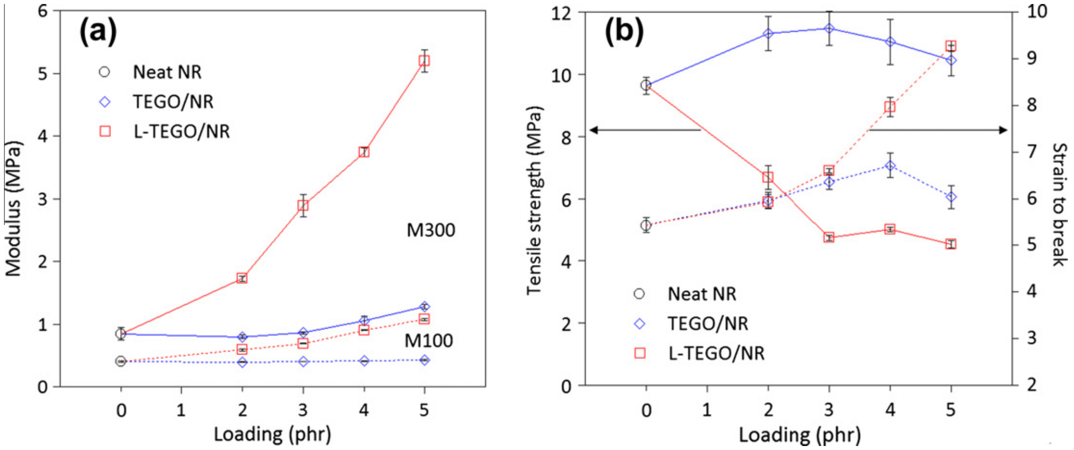

Fig. 4. Summary of (a) modulus data and (b) strength and elongation data of the nanocomposites. M100 and M300 represent modulus at 100% elongation and 300% elongation, respectively, as determined by ASTM D412.

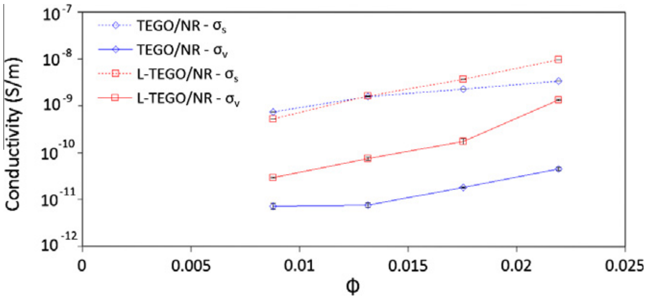

Fig. 5. Electrical conductivity of TEGO/NR and L-TEGO/NR nanocomposites as a function of volume fraction of TEGO, ϕ. Solid lines indicate volumetric conductivity data (σ_v; through-plane) and dashed lines indicate sheet conductivity data (σ_s; in-plane).

particularly evident in the L-TEGO/NR Mooney–Rivlin curves. This comparison is further evidence for a better dispersion of filler in the L-TEGO/NR samples as described in Section 3.3.

3.3. Nanocomposite morphological evaluation and composite theory analysis

Based on the property measurements presented in Section 3.2, it was expected that morphological characterization via WAXS and TEM would reveal an improved dispersion in the L-TEGO/NR nanocomposites compared with the TEGO/NR nanocomposites. As shown in the Supporting Information (Fig. A2), no evidence of a graphite or GO peak was observed in the WAXS spectra, suggesting an exfoliated morphology in both types of nanocomposites.

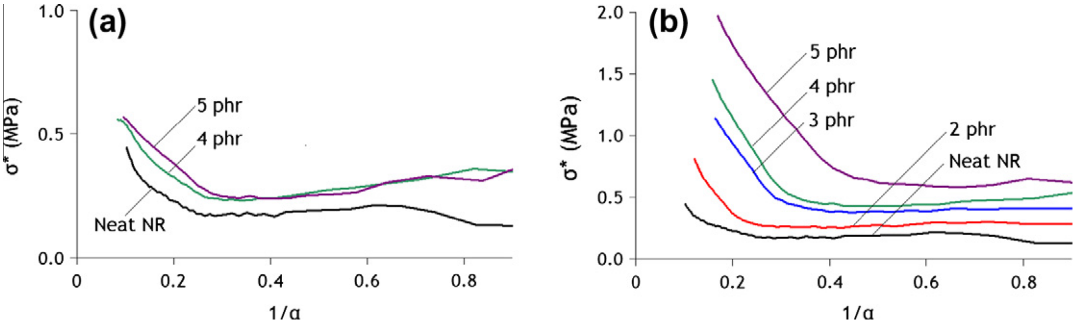

Fig. 6. Mooney–Rivlin plots of (a) TEGO/NR and (b) L-TEGO/NR nanocomposites (curves for 2 and 3 phr TEGO/NR nanocomposites not included for clarity).

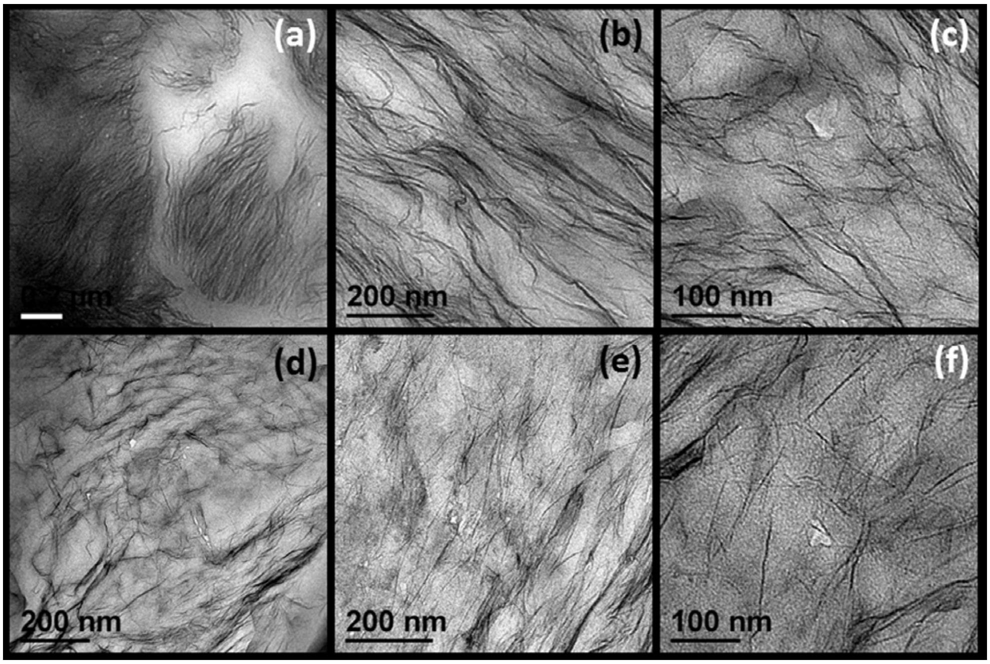

Fig. 7. TEM micrographs of (a), (b), and (c), TEGO/NR and (d), (e), and (f) L-TEGO/NR nanocomposites. Scale bar in image (a) is 200 nm.

TEM micrographs of thin sections of the nanocomposites are presented in Fig. 7 and show some clear differences in the dispersions. TEGO/NR micrographs revealed significant variation in the dispersion over the cross section—some regions showed highly-exfoliated, randomly-oriented platelets while others showed large particles consisting of bundles of platelets (see Figs. 7a and Fig. A5). Many platelets exhibited wrinkled conformations, consistent with the disordered structure observed by SEM (Fig. 2) and other observations on TEGO and TEGO-filled polymers [6,7]. By comparison, the L-TEGO/NR nanocomposites exhibited a more uniform dispersion state, with far fewer unexfoliated TEGO particles. In addition, the platelets appeared less wrinkled in the L-TEGO/NR nanocomposites, perhaps because the dispersion of TEGO into pH 11 water by sonication could flatten out the corrugated platelets due to ionization of residual functional groups [19]. Evidently the ultrasonic treatment, despite not achieving a stable suspension of individual TEGO platelets, promotes breakup of large particles and facilitates the dispersion of few-layer TEGO platelets into the NR matrix.

We sought to quantify the apparent improvement in dispersion in terms of an average aspect ratio of platelets, A_f. We recently presented a comprehensive discussion on dispersion quantification of graphene platelets in NR [12] and extended that analysis to this work to determine A_f of the two types of nanocomposites. Fig. 8 presents a histogram of A_f values determined from several TEM images at various magnifications for both types of nanocomposite at 5 phr loading (see Fig. A6 for an illustration of the procedure). As with our previous work with RG-O/NR nanocomposites, the amount of disorientation and platelet overlap made identification of individual platelets challenging, and thus the average A_f values may only represent a rough estimate [20]. Still, despite the tremendous dispersion enhancement suggested by the property measurements, similar average A_f values were determined from TEM analysis for the two types of nanocomposites—34 for TEGO/NR, compared with 38 for L-TEGO/NR. Even in light of the challenges in the procedure for quantifying dispersion [20], the small disparity in A_f between the two types of nanocomposites suggests that the stark difference in mechanical properties cannot simply be attributed to more effective load bearing by higher aspect ratio particles.

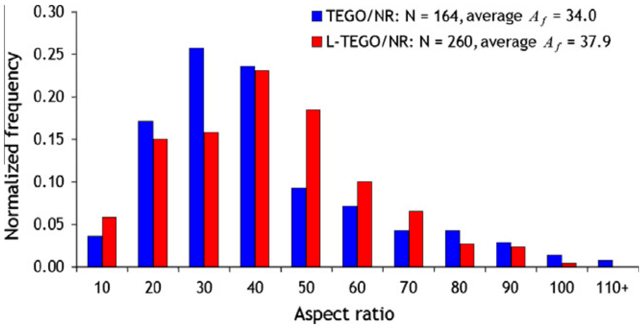

Fig. 8. Histogram showing A_f values of TEGO platelets determined by image analysis of representative TEM images of TEGO/NR and L-TEGO/NR nanocomposites.

Indeed, closer inspection of the micrographs suggests that while the particle/tactoid aspect ratios may be similar, the average lateral and thickness dimensions of the individual platelets are not. The average platelet thicknesses and lateral dimensions were 2.0 nm and 77.6 nm for L-TEGO/NR, and 5.7 nm and 194 nm for TEGO/NR, respectively. Calculations of surface area to volume ratio at a fixed volume show that, assuming a perfect dispersion, the amount of interfacial surface area per unit volume is higher in the L-TEGO/NR nanocomposites by a roughly a factor of 3. This difference is likely greater as the presence of closely-spaced and overlapping platelets required some platelets to be excluded from the analysis. Tactoids consisting of many parallel, closely-spaced platelets would lower the average A_f if considered as a single particle, and such a morphology would be less effective for reinforcement compared with well-exfoliated and homogeneously-dispersed platelets as it would restrict the ability of the chains to adsorb onto the platelet surface [20]. The impact of a higher amount of accessible interfacial surface area on mechanical properties can be qualitatively understood using the concept of “bound rubber” in which chains adsorbed onto the surface of TEGO platelets are immobilized and therefore increase the effective volume fraction of filler [3], enhancing the strain amplification effect [21] of the filler and

Table 1
Aspect ratio predictions of composite models based upon experimental initial modulus data.

Model	A_f – TEGO/NR	A_f – L-TEGO/NR
Guth equation	22	39
Modified Halpin–Tsai	18	47
Mori–Tanaka	33	90

promoting strain-induced crystallization at lower applied strains. Thus while the average platelet A_f of the two dispersions were similar, the larger amount of accessible interfacial surface area and more uniform dispersion in the L-TEGO/NR nanocomposites could be largely responsible for the difference in mechanical properties between the two types of nanocomposites. Additionally, as enhancement in conductivity is largely governed by percolation of conductive platelets [17,18], the large gaps between tactoids evident in, e.g., Fig. 8a, could be largely responsible for the differences in thermal and electrical conductivity between the two types of nanocomposites.

The average A_f determined by TEM analysis was compared with composite models that exhibited close agreement with experimental data on RG-O/NR nanocomposites [12]; further details on the calculations are provided in the Supporting Information. As shown in Table 1, in this study good agreement between the Guth equation prediction and experimental modulus data was obtained when taking the shape factor f equal to A_f as determined from TEM analysis. The A_f of TEGO/NR nanocomposites determined by TEM analysis was larger than the predictions of any of the models investigated here, however. This could be due to the nature of the dispersion, consisting of high aspect ratio platelets arranged in a morphology roughly corresponding to an intercalated structure [1].

3.4. Comparison of TEGO and carbon black-filled NR

What advantage, if any, do graphene-based fillers provide over carbon black, the most widely-used reinforcing filler material? Table 2 summarizes the properties of TEGO and CB-filled NR nanocomposites at 5 phr loading. Properties of RG-O/NR nanocomposites produced by latex co-coagulation [12], subjected to a similar milling procedure and cured with 1 phr DCP, are also presented for reference. Clearly, despite the dramatic property enhancement conferred by the latex pre-mixing procedure, the mechanical property improvements of the L-TEGO/NR nanocomposites were considerably smaller than achieved with the RG-O/NR nanocomposites. Mechanical property enhancements with CB were comparable to, if not better than, TEGO when dispersed into NR directly on a two-roll mill. CB also provided larger enhancement in thermal conductivity than any of the graphene-based fillers, although it provided the lowest enhancement in electrical conductivity. This result may be explained in part by observations that the thermal conductivity decreases with increasing modulus contrast between the matrix and filler, due to increasing Kapitza resistance [22–24]. The greater modulus and aspect ratio of TEGO platelets compared with CB could thus provide greater reinforcement and electrical conductivity enhancement (as higher aspect ratio promotes filler percolation), at the cost of relatively smaller thermal conductivity enhancement.

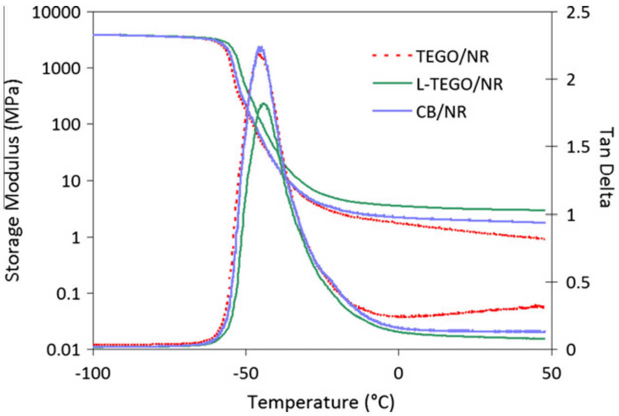

Fig. 9. Dynamic mechanical analysis plots from temperature scans on the nanocomposites.

Fig. 9 shows results from DMA temperature scans on the nanocomposites. TEGO, L-TEGO, and CB-filled NR all showed similar average values of glassy modulus (approximately 3.8 GPa) and similar average glass transition temperature (T_g) values (-44 to -46 °C), with the L-TEGO/NR samples showing the largest modulus in the rubbery region above T_g. All nanocomposites showed a decreased $\tan\delta$ peak height and breadth versus neat NR, suggesting strong interfacial bonding between the matrix and filler [25]. L-TEGO/NR nanocomposites exhibited the smallest $\tan\delta$ peak, reflecting the better dispersion of filler and higher accessible interfacial surface area in those samples.

4. Conclusions

Two-roll mill processing was used to disperse thermally expanded graphite oxide (TEGO) into natural rubber (NR). Property improvements achieved by direct milling of TEGO into NR were small and comparable to those provided by carbon black; however, by pre-mixing TEGO with NR latex followed by milling, substantial property enhancements were achieved. As quantitative TEM analysis suggested a small difference in dispersion in terms of an average platelet aspect ratio, we attributed the large property improvements in the L-TEGO/NR nanocomposites to a more uniform dispersion of TEGO platelets, coupled with a larger accessible interfacial surface area.

While ultrasonic treatment of TEGO in water does not produce a stable suspension of exfoliated TEGO platelets, it does serve to break down the particles and facilitates the dispersion of high aspect ratio platelets into the NR matrix during milling. These results suggest that effective dispersion of TEGO into NR using conventional rubber processing equipment, without the use of solvents or pre-mixing with latex, could pose a significant challenge.

Table 2
Property comparison of NR-matrix nanocomposites with different fillers at five phr loading. (Standard error of measurements omitted for clarity. Thermal conductivity represented by k, σ_v represents volumetric conductivity, and σ_s represents sheet conductivity. RG-O platelets were dispersed into NR by a latex co-coagulation method.)

Filler	M100 (MPa)	M300 (MPa)	σ_t (MPa)	Strain at break	k (W/m K)	σ_v (S/m)	σ_s (S/m)
TEGO	0.43	1.28	6.05	8.96	0.166	4.50×10^{-11}	3.41×10^{-9}
L-TEGO	1.07	5.19	10.90	5.03	0.180	1.32×10^{-9}	9.69×10^{-9}
CB	0.51	1.19	6.28	8.34	0.228	6.73×10^{-12}	5.36×10^{-10}
RG-O	1.59	9.01	10.18	3.19	0.190	5.10×10^{-6}	7.91×10^{-7}
Neat NR	0.41	0.84	5.15	8.44	0.157	6.72×10^{-16}	1.97×10^{-13}

Acknowledgements

The authors would like to thank D.R. Paul for use of the two-roll mill and hot press, K.M. Liechti for assistance with and use of an MTS machine for stress-strain testing, W. Li and X. Kim for DMA use, C. Pulford and X. Yang at Goodyear for helpful advice, and D. Romanovicz for cryomicrotome training. This project was funded in part by the Goodyear Tire and Rubber Company and by the Laboratory Directed Research and Development (LDRD) program and the National Institute for Nano-Engineering at Sandia National Laboratories (NINE).

Appendix A. Supplementary material

Supplementary data associated with this article can be found, in the online version, at http://dx.doi.org/10.1016/j.compscitech.2012.11.008.

References

[1] Potts JR, Dreyer DR, Bielawski CW, Ruoff RS. Graphene-based polymer nanocomposites. Polymer 2011;52:5–25.
[2] Zhan YH, Wu JK, Xia HS, Yan N, Fei GX. Dispersion and exfoliation of graphene in rubber by an ultrasonically-assisted latex mixing and in situ reduction process. Macromol Mater Eng 2011;296:590–602.
[3] Ozbas B, Toki S, Hsiao BS, Chu B, Register RA, Aksay IA, et al. Strain-induced crystallization and mechanical properties of functionalized graphene sheet-filled natural rubber. J Polym Sci Part B: Polym Phys 2012;50:718–23.
[4] Park S, Ruoff RS. Chemical methods for the production of graphenes. Nat Nanotechnol 2009;5(4):217–24.
[5] Ruess VG, Vogt F. Monatsh Chem 1948;78:222–42.
[6] Schniepp HC, Li JL, McAllister MJ, Sai H, Herrera-Alonso M, Adamson DH, et al. Functionalized single graphene sheets derived from splitting graphite oxide. J Phys Chem B 2006;110(17):8535–9.
[7] Zhu YW, Murali S, Stoller MD, Velamakanni A, Piner RD, Ruoff RS. Microwave assisted exfoliation and reduction of graphite oxide for ultracapacitors. Carbon 2010;48(7):2118–22.
[8] Kim H, Abdala AA, Macosko CW. Graphene/polymer nanocomposites. Macromolecules 2010;43:6515–30.
[9] Potts JR, Murali S, Zhu Y, Zhao X, Ruoff RS. Microwave-exfoliated graphite oxide/polycarbonate composites. Macromolecules 2011;44:6488–95.
[10] Potts JR, Lee SH, Alam TM, An J, Stoller MD, Piner RD, et al. Thermomechanical properties of chemically modified graphene/poly(methyl methacrylate) composites made by in situ polymerization. Carbon 2011;49:2615–23.
[11] Kim H, Miura Y, Macosko CW. Graphene/Polyurethane nanocomposites for improved gas barrier and electrical conductivity. Chem Mater 2010;22(11):3441–50.
[12] Potts JR, Shankar O, Du L, Ruoff RS. Processing-morphology-property relationships and composite theory analysis of reduced graphene oxide/natural rubber nanocomposites. Macromolecules 2012;45:6045–55.
[13] Mark JE, Erman B, Eirich FR, editors. The science and technology of rubber. Elsevier; 2010.
[14] Harwood JAC, Payne AR. Stress softening in natural rubber vulcanizates. Part IV. Unfilled vulcanizates. J Appl Polym Sci 1966;10:1203–11.
[15] McAllister MJ, Li JL, Adamson DH, Schniepp HC, Abdala AA, Liu J, et al. Single sheet functionalized graphene by oxidation and thermal expansion of graphite. Chem Mater. 2007 Sep;19(18):4396–404.
[16] Qureshi MN, Qammar H. Mill processing and properties of rubber–clay nanocomposites. Mater Sci Eng C 2010;30:590–6.
[17] Bauhofer W, Kovacs JZ. A review and analysis of electrical percolation in carbon nanotube polymer composites. Compos Sci Technol 2009;69(10):1486–98.
[18] Nan C-W, Shen Y, Ma J. Physical properties of composites near percolation. Annu Rev Mater Res 2010;40:131–51.
[19] Ma X, Zachariah MR, Zangmeister CD. Crumpled nanopaper from graphene oxide. Nano Lett 2012;12:486–9.
[20] Fornes TD, Paul DR. Modeling properties of nylon 6/clay nanocomposites using composite theories. Polymer 2003;44(17):4993–5013.
[21] Mullins L, Tobin NR. Stress softening in rubber vulcanizates. Part I. Use of a strain amplification factor to describe the elastic behavior of filler-reinforced vulcanized rubber. J Appl Polym Sci 1965;9:2993–3009.
[22] Cui W, Du F, Zhao J, Zhang W, Yang Y, Xie X, et al. Improving thermal conductivity while retaining high electrical resistivity of epoxy composites by incorporating silica-coated multi-walled carbon nanotubes. Carbon 2011;49:495–500.
[23] Clancy TC, Gates TS. Modeling of interfacial modification effects on thermal conductivity of carbon nanotube composites. Polymer 2006;47:5990–6.
[24] Peters JE, Papavassiliou DV, Grady BP. Unique thermal conductivity behavior of single-walled carbon nanotube-polystyrene composites. Macromolecules 2008;41:7274–7.
[25] Galimberti M, editor. Rubber–clay nanocomposites. Hoboken, New Jersey: John Wiley & Sons; 2011.